Available online at www.sciencedirect.com
ScienceDirect
European Journal of Mechanics B/Fluids 27 (2008) 501–513

Global two-dimensional stability measures of the flat plate boundary-layer flow

Espen Åkervik [a], Uwe Ehrenstein [b], François Gallaire [c], Dan S. Henningson [a,*]

[a] *Linné Flow Centre, KTH Mechanics, SE-100 44 Stockholm, Sweden*
[b] *IRPHÉ, Université de Provence, F-13384 Marseille Cedex 13, France*
[c] *Laboratoire J.A. Dieudonné, Parc Valrose, F-06108 Nice Cedex 02, France*

Received 30 March 2007; received in revised form 8 August 2007; accepted 24 September 2007

Available online 4 October 2007

Abstract

The stability of the two-dimensional flat plate boundary-layer is studied by means of global eigenmodes. These eigenmodes depend both on the streamwise and wall-normal coordinate, hence there are no assumptions on the streamwise length scales of the disturbances. Expanding the perturbation velocity field in the basis of eigenmodes yields a reduced order model from which the stability characteristics of the flow, i.e. the initial condition and forcing function leading to the largest energy growth, are extracted by means of non-modal analysis. In this paper we show that, even when performing stability analysis using global eigenmodes, it is not sufficient to consider only a few of the least damped seemingly relevant eigenmodes. Instead it is the task of the optimization procedure, inherent in the non-modal analysis, to decide which eigenmodes are relevant. We show that both the optimal initial condition and the optimal forcing structure have the form of upstream tilted structures. Time integration reveals that these structures gain energy through the so called Orr mechanism, where the instabilities extract energy from the mean shear. This provides the optimal way of initiating Tollmien–Schlichting waves in the boundary layer. The optimal initial condition results in a localized Tollmien–Schlichting wavepacket that propagates downstream, whereas the optimal forcing results in a persistent Tollmien–Schlichting wave train.

Keywords: Boundary layer stability; Global modes; Convective instabilities; Non-modal stability

Boundary layers, jets and mixing layers are examples of convectively unstable flows, where disturbances are amplified while being advected downstream. In these configurations, the flow relaxes in the absence of external disturbances. For certain parameter ranges, for example if the reversed flow in separated boundary layers becomes large, the flow might become absolutely unstable. Instead of constantly requiring external input to maintain the flow disturbances, pockets of absolutely unstable regions support self-sustained oscillations. Following a phase of linear growth of the global mode, there is a saturation into a non-linear limit cycle with the absolutely unstable flow domain acting as a wave maker shedding vorticity into the convectively unstable region. When the flow under consideration is slightly non-parallel it is possible to determine criteria for transition from globally stable, to convectively unstable and finally

* Corresponding author.
E-mail address: henning@mech.kth.se (D.S. Henningson).

0997-7546/$ – see front matter
doi:10.1016/j.euromechflu.2007.09.004

to absolutely unstable based on classical local analysis [1]. In local analyses the streamwise and spanwise directions of the flow are taken to be homogeneous, yielding eigenvalue problems depending only on the wall normal direction. When the length scales of the disturbances becomes comparable to those of the base flow, which is the case for highly non-parallel flows, it is clear that one has to resort to a global formulation of the stability problem, treating also the streamwise direction as inhomogeneous. The resulting matrix eigenvalue problem is typically very large, but owing to increased computer capabilities and efficient large scale eigenvalue solving strategies based on Krylov methods, it is nowadays tractable to compute global eigenmodes for many flow cases.

As the relevance of global analysis is well established for highly non-parallel flows [2], there are still some important issues to be dealt with when it comes to applying this methodology to slightly non-parallel situations. Considering the model problem provided by the Ginzburg–Landau equation with spatially varying coefficients, Cossu and Chomaz [3] demonstrated that the non-normality of the streamwise eigenmodes leads to transient growth. This non-normality is considered to be associated with the streamwise separation of the direct and adjoint global modes due to the basic advection [4]. Schmid and Henningson [5] advocated the robustness of optimally summing the streamwise eigenmodes when studying a model problem for a falling liquid curtain. They showed that the sum of modes, in contrast to single modes, yielded results in agreement with experiments. The use of global modes as a tool for studying the stability characteristics of the slightly non-parallel boundary-layer flow was addressed in Ehrenstein and Gallaire [6]. They found that a superposition of the damped global eigenmodes associated with Tollmien–Schlichting (TS) type of structures gave rise to a localized wavepacket at the inflow boundary. The wavepacket would grow while being advected downstream, in close agreement with direct numerical simulation results.

It is now well accepted that when incoming disturbances exceed a certain amplitude threshold the flat-plate boundary layer is likely to undergo transition due to three-dimensional instabilities through the lift-up effect [7,8]. This transient growth scenario, where streamwise vortices form into streamwise streaks by the action of the mean flow, was studied for a variety of shear flows in the locally parallel assumption (cf. [9–11]). The extension to the non-parallel flat plate boundary layer was performed at the same time by Luchini [12] and Andersson et al. [13] marching the parabolized stability equations in the streamwise direction.

While emphasizing the strength of three-dimensional disturbances in general shear flows, Butler and Farrell [9] found a two-dimensional instability mechanism not related to the TS-waves. This instability could extract energy from the mean shear by transporting momentum down the mean momentum gradient through the action of the perturbation Reynolds stress. This means that structures that are tilted against the shear, will first rise to an upright position while borrowing energy from the mean flow, after which the energy is returned to the mean flow and the disturbances decay. They referred to this as the Reynolds stress mechanism, commonly also known as the Orr mechanism.

In this paper we re-address two-dimensional stability mechanisms in the flat-plate boundary-layer flow, by considering the cooperation or competition of the wall-normal non-normal effects responsible for the Orr mechanism and the streamwise non-normal effects triggering the TS-waves, bearing in mind that the latter are the building blocks for the onset of the so-called classical transition in a low-level noise environment [14]. The analysis is based on the computation of temporal two-dimensional modes and is hence free from any assumption concerning spatial length-scales. The non-normality of these eigenmodes of the linearized Navier–Stokes operator is shown to lead to large energy gain due to combination of the Orr and TS mechanisms.

The paper is organized as follows. Section 2 is devoted to the description of the numerical tools. Convergence results of the global eigenvalue spectrum are provided in Section 3. The optimal initial condition leading to the maximum energy gain is computed and discussed in Section 4. The signalling problem, that is the determination of the optimal harmonic forcing distribution of the Navier–Stokes system in a Direct Numerical Simulation sense (DNS), is addressed in Section 5. In particular, the disturbance flow evolution obtained through projection on the set of global eigenmodes is compared to the forced Navier–Stokes dynamics. Some conclusions are provided in Section 6.

1. Numerical tools

1.1. Basic state

The Navier–Stokes equations are solved by means of direct numerical simulation (DNS), both in order to obtain a steady state base flow for linearization and to compute the evolution of disturbances on top of this base flow. The Reynolds number $Re = U_\infty \delta^*/\nu = 1000$ is based on the freestream velocity U_∞, the displacement thickness δ^* at

inflow $x = 0$ and the kinematic viscosity ν. All variables are made dimensionless with U_∞ and δ^*. The computational domain is $0 \leqslant x \leqslant 1000$, $0 \leqslant y \leqslant 80$. At inflow a Blasius profile is prescribed and at outflow a classical advection condition is imposed. No slip condition is enforced at the wall $y = 0$ whereas at the top $y = 80$ the flow is freestream uniform, i.e. the streamwise velocity component is $u = U_\infty$ and the wall normal component is $v = 0$. The DNS procedure has previously been used in [6]. The flow variables are discretized using fourth-order finite differences in streamwise direction (with 5120 grid points) and Chebyshev-collocation in the vertical direction (with 97 collocation points). The steady state $\mathbf{U} = (U(x, y), V(x, y))$ and $P(x, y)$ is obtained by integrating the Navier–Stokes in time by means of the DNS.

1.2. Two-dimensional temporal modes

By splitting the total flow field into a mean and a perturbation/fluctuating part $\mathbf{U} + \mathbf{u}$ and $P + p$ and by linearizing the Navier–Stokes equations about the base flow one can easily recognize that the disturbance flow field with velocity components $\mathbf{u}(x, y, t)$ and pressure field $p(x, y, t)$ satisfy the partial differential equations

$$\begin{aligned} \frac{\partial \mathbf{u}}{\partial t} &= -(\mathbf{U}\cdot\boldsymbol{\nabla})\mathbf{u} - (\mathbf{u}\cdot\boldsymbol{\nabla})\mathbf{U} - \boldsymbol{\nabla} p + \frac{1}{Re}\boldsymbol{\nabla}^2\mathbf{u}, \\ 0 &= \boldsymbol{\nabla}\cdot\mathbf{u}. \end{aligned} \tag{1}$$

After discretization in the space variables this system can be written

$$\frac{\mathrm{d}}{\mathrm{d}t}\mathbf{B}\mathbf{q} = \mathbf{A}\mathbf{q}, \tag{2}$$

where $\mathbf{q} = [\mathbf{u}, p]^T$ and $\mathbf{B}$ is the projection of the total disturbance field $\mathbf{q}$ on its velocity components, i.e. $\mathbf{B}\mathbf{q} = [\mathbf{u}, 0]$. Note that in (2) a divergence-free velocity field trivially satisfies $\mathbf{B}\mathbf{A}\mathbf{q} = \mathbf{A}\mathbf{q}$. Taking the exponential Ansatz for the time dependence $\mathbf{q}(x, y, t) = \tilde{\mathbf{q}}(x, y)\mathrm{e}^{-\mathrm{i}\omega t}$ yields the generalized eigenvalue problem

$$-\mathrm{i}\omega_l \mathbf{B}\tilde{\mathbf{q}}_l = \mathbf{A}\tilde{\mathbf{q}}_l \tag{3}$$

with a divergence free velocity field $\tilde{\mathbf{u}}_l$ associated to each eigenmode $\tilde{\mathbf{q}}_l$. The computational domain used for the eigenmode calculations is $0 \leqslant x \leqslant L_x$, $0 \leqslant y \leqslant L_y$. In the wall normal y-direction a height of $L_y = 40$ was found sufficient to also resolve the eigenvectors associated with the low frequency part of the spectra. In the streamwise x-direction different lengths L_x have been considered, but the main parts of the results are presented for $L_x = 800$. Indeed the flat-plate boundary layer flow is convectively unstable and the box length will set a bound on the timescale at which the spatially growing disturbance wavepacket leaves the domain. Accordingly, the eigenmodes and the instability mechanisms will also be function of the box length. At the wall and at free-stream homogeneous Dirichlet conditions are imposed and at inflow and outflow the non-homogeneous Robin conditions proposed in [6] have been used. These boundary conditions essentially amount to matching the streamwise derivative of the global mode with spatial local analysis so that $\partial\mathbf{u}/\partial x = i\alpha\mathbf{u}$. The local dispersion relation connecting the wave number α to the frequency ω is non-linear, but performing a Gaster-type of transformation

$$\alpha \approx \alpha_{0,r} + \frac{\partial \alpha_r}{\partial \omega_r}(\omega_0)(\omega - \omega_0)\cdots \tag{4}$$

yields a good linear approximation, as long as the imaginary parts of the complex frequency and wavenumber are small. Here the real frequency ω_0 is chosen such that $\alpha_0 = \alpha_{0,r}$ at the inflow boundary, that is at a frequency of neutral instability for the Blasius profile at inflow. Fig. 1 shows the real part of the complex wavenumber α_r as function of the real frequency, as provided by the local dispersion relation for the Blasius profile at inflow $Re = 1000$, which is indeed close to its linear approximation (4) depicted as the dotted line. The domain is mapped into $[-1, 1] \times [-1, 1]$ and a Chebyshev–Chebyshev collocation discretization is used for the stability system. Chebyshev-collocation provides the most efficient discretization in terms of grid size, which puts a reasonable bound on the dimension of the resulting generalized matrix eigenvalue problem. Consequently, the basic steady flow computed by means of DNS is interpolated on the new grid (cf. [6] for details). We have chosen to consider the steady state for the Navier–Stokes system, rather than the self-similar solution of the flat-plate boundary-layer equations. One goal of the present analysis is to compare the Navier–Stokes dynamics with the time evolution of the eigenmodes system. It

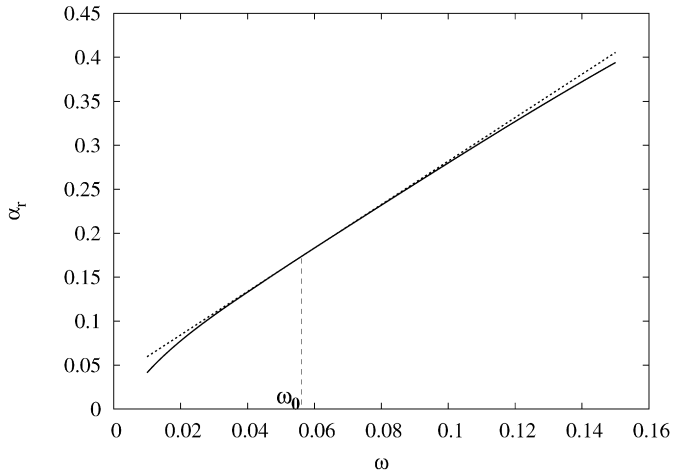

Fig. 1. Real part of the wavenumber α_r. Solid line shows the α_r as provided by the local dispersion relation for the Blasius profile at inflow $Re = 1000$, and the dotted line shows the linear approximation as given by the Gaster-type of approximation (4).

will be shown in Section 3 that a collocation grid with 250×45 collocation points yields converged stability results. The resulting eigenvalue problem is still far too large to be solved by standard QZ algorithms. Large-scale Krylov subspace projections with dimension $m = 2000$ together with the Arnoldi algorithm [15] proved suitable to provide a complete, with respect to the disturbance dynamics, set of eigenvalues and corresponding eigenmodes.

1.3. Mode superposition

When determining the possibility of growth in a flow system the notions of optimal initial condition and optimal forcing are essential. These features are both closely related to the non-normality of the underlying operators [16]. We will here give a brief summary on how these optima are computed. The dynamical system (2) obtained after discretization defines an initial value problem by adding the initial condition

$$\mathbf{u}(0) = \mathbf{u}_0 \tag{5}$$

for a divergence-free velocity field $\mathbf{u}_0$. We are looking for initial disturbances that maximize the energy at time t

$$G(t) = \max_{\mathbf{u}_0 \neq 0} \frac{\|\mathbf{u}(t)\|_E^2}{\|\mathbf{u}_0\|_E^2}$$

and a convenient form of this expression can be obtained by expanding the solution in terms of the generalized eigenmodes $\mathbf{u}(t) = \sum_{l=1}^{N} \kappa_l(t)\tilde{\mathbf{u}}_l$. Recall that the eigenmodes are the solutions to the generalized eigenvalue problem (3). Keeping in mind that the pressure acts as Lagrange multiplier in order to maintain divergence free velocity fields, the flow dynamics is then determined purely by the velocity components of the eigenmodes. Hence the flow dynamics is described by

$$\frac{\mathrm{d}\mathbf{k}}{\mathrm{d}t} = \boldsymbol{\Lambda}\mathbf{k}, \quad \mathbf{k}(0) = \mathbf{k}_0, \tag{6}$$

where $\mathbf{k} = [\kappa_1, \kappa_2, \ldots, \kappa_N]$ is the vector of expansion coefficients and $\boldsymbol{\Lambda}$ is a diagonal matrix whose elements are given by $\Lambda_{ll} = -\mathrm{i}\omega_l$. The flow perturbation energy in this basis is $\|\mathbf{u}\|_E^2 = \|\mathbf{F}\exp(\boldsymbol{\Lambda}t)\mathbf{k}_0\|_2^2$, where F is the Cholesky factor of the Hermitian energy measure matrix $\mathbf{M}$ with entries $M_{ij} = \int \tilde{\mathbf{u}}_i^H \tilde{\mathbf{u}}_j \,\mathrm{d}x\,\mathrm{d}y$. Hence, the maximum growth expressed in the basis of eigenmodes reads

$$G(t) = \|\mathbf{F}\exp(\boldsymbol{\Lambda}t)\mathbf{F}^{-1}\|_2^2. \tag{7}$$

The largest growth at time t is given by the largest singular value of $\mathbf{F}\exp(\boldsymbol{\Lambda}t)\mathbf{F}^{-1}$ and the optimal initial condition is $\mathbf{k}_0 = \mathbf{F}^{-1}\mathbf{z}$, where $\mathbf{z}$ is the right singular vector. Alternative ways of computing the optimal initial condition are by calculus of variations [9] or by time-marching/space-marching algorithms involving the adjoint operator [12,13].

Let us now formulate the optimal forcing frequency and the corresponding forcing function. Consider the harmonically forced system

$$\frac{\partial}{\partial t}\mathbf{B}\mathbf{q} = \mathbf{A}\mathbf{q} + \{\mathbf{q}_f \exp(-\mathrm{i}\Omega t)\}, \quad \Omega \text{ real.} \tag{8}$$

The asymptotic long time response for the stable system reads

$$\mathbf{q}_r(t) = -(\mathbf{A} + \mathrm{i}\Omega\mathbf{B})^{-1}\mathbf{q}_f \exp(-\mathrm{i}\Omega t). \tag{9}$$

Expressing the state in the basis of eigenmodes yields

$$\mathbf{k}_r(t) = -(\boldsymbol{\Lambda} + \mathrm{i}\Omega\mathbf{I})^{-1}\mathbf{k}_f \exp(-\mathrm{i}\Omega t). \tag{10}$$

The maximum response to the harmonic forcing at a frequency Ω expressed in this basis is

$$R(\Omega) = \max_{\mathbf{q}_f} \frac{\|\mathbf{q}_r\|_E}{\|\mathbf{q}_f\|_E} = \left\|\mathbf{F}(\boldsymbol{\Lambda} + \mathrm{i}\Omega\mathbf{I})^{-1}\mathbf{F}^{-1}\right\|_2. \tag{11}$$

The norm of the resolvent is readily obtained as the largest singular value of $\mathbf{F}(\boldsymbol{\Lambda} + \mathrm{i}\Omega\mathbf{I})^{-1}\mathbf{F}^{-1}$ and the optimal forcing $\mathbf{k}_f$ is retrieved from the right singular vector $\mathbf{z}$ through the expression $\mathbf{k}_f = \mathbf{F}^{-1}\mathbf{z}$. In a similar manner the asymptotic response can be obtained from the left singular vector.

Two different contributions to large resolvent norms may be identified: resonances are triggered whenever the forcing frequency is chosen close to an eigenvalue of the system. On the other hand, the optimal forcing may exploit the large condition number of $\mathbf{F}$, related to the non-orthogonality of the eigenvectors.

2. The spectra and convergence of optima

2.1. Global spectra and mode structures

Fig. 2 shows the spectra obtained for the inflow Reynolds number $Re = 1000$ displayed as stars. The box size of $L_x = 800$, $L_y = 40$ required $N_x = 250$ and $N_y = 45$ in order to yield converged results. The largest Krylov subspace size considered is $m = 2000$. We found that increasing the number of points in both the streamwise and wall-normal

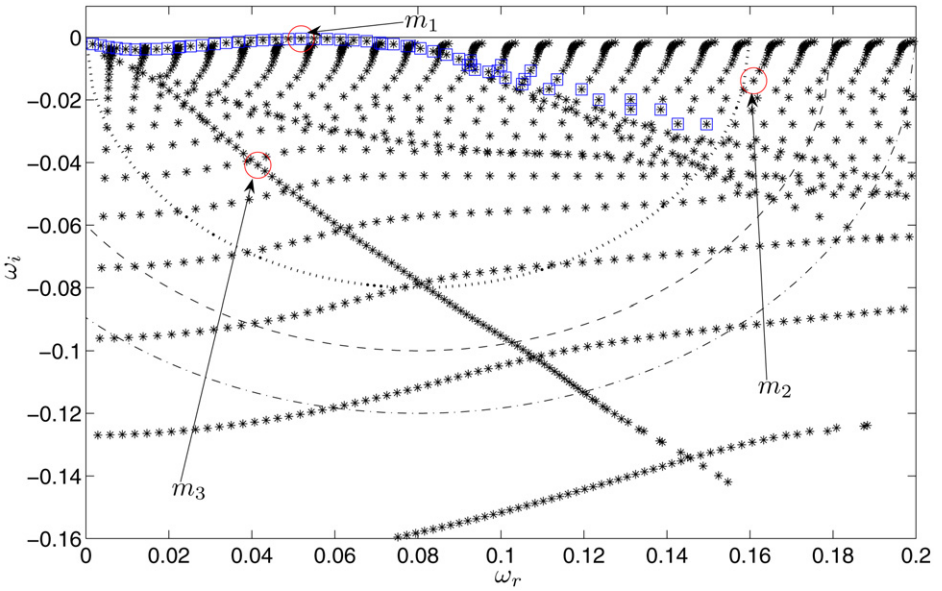

Fig. 2. Stars show spectra at $Re = 1000$. Included are also contours in the complex plane indicating size of Krylov subspace according to $|\omega - \sigma_0| < R$. (...) shows $R = 0.08$, (___) shows $R = 0.1$ and (_._) shows $R = 0.12$. Eigenvectors corresponding to labels m_1, m_2 and m_3 are depicted in Fig. 3. Note especially that m_1 represents the TS type of eigenmodes, whereof the others are enclosed by squares.

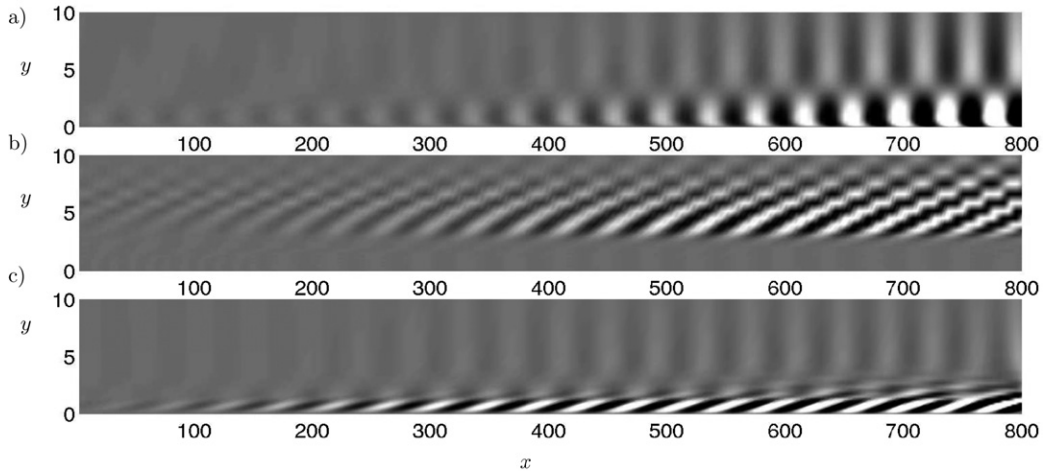

Fig. 3. Streamwise component of eigenvectors corresponding to the eigenvalues labelled m_1 to m_3 in Fig. 2. (a) (m_1) Least stable TS type of mode. (b) (m_2) Mode associated with the wall normal continuous branch. (c) (m_3) Orr type of mode. The last two are typical modes that due to cancelling with other non-orthogonal modes contribute to the Orr mechanism. Note that the domain is truncated at $y = 10$ for visualization purposes.

direction only moved the most damped eigenvalues, associated with areas of a resolvent norm of the order of 10^6 [17]. As can be observed from the figure, there are many eigenmodes obtained by the eigenvalue calculation. We can identify several branches which all can be related to the spectrum of a parallel Blasius boundary layer, as found by solving the Orr–Sommerfeld equations, though modified by non-parallelism and boundary conditions.

From Fig. 2 one can observe that there is a branch of the global spectra which is identifiable as TS waves. This branch is marked with squares. The mode labelled m_1 is the least stable eigenmode for this specific box. In Fig. 3(a) the spatial structure of the streamwise velocity component of this eigenfunction is shown. The TS type of eigenfunctions have wall normal profiles that match the ones obtained from the OS equation, however with the difference that the global eigenfunctions are spatially evolving downstream. As shown in Ehrenstein and Gallaire [6], the global eigenfunctions exhibit a spatial growth that locally match weakly non-parallel TS waves at the corresponding global eigenfrequency.

The modes labelled m_2 in Fig. 2 reach their maximum in the free stream and are reminiscent of the continuous spectrum of the local Orr–Sommerfeld analysis of a Blasius boundary layer flow. In the latter case the phase speed ω_r/α_r is close to the free stream velocity. In our non-parallel framework, since α_r is not prescribed, the modes are aligned on a series of equidistant distorted S shapes.

The eigenmode labelled m_3 is representative of a wall normal discrete damped branch. From Fig. 3(c) it can be seen that the eigenfunction displays downstream tilted structures with an amplitude maximum inside the boundary layer. One might call these eigenmodes Orr modes, given their tilted structure, reminiscent of late stages of the Orr mechanism.

Let us further compare our global non-parallel analysis to the well-known stability analysis of the parallel Blasius flow studied by means of the Orr–Sommerfeld equation. Such a comparison is not straightforward, since for each local position, and for each axial wavenumber, a full discrete and continuous spectrum is retrieved from the Orr–Sommerfeld equation. We found that the best comparison could be done at the position $x = 300$, corresponding to a local Reynolds number of $Re = 1374$. In Fig. 4(a) we have represented some temporal stability branches of the discrete Orr–Sommerfeld spectrum, as they evolve when the axial wavenumber is continuously varied.

More precisely, we depict as continuous lines in Fig. 4(a) the trace of the TS branch and two damped branches of the Orr–Sommerfeld equations as the wave number is varied. One can clearly see that global and local analysis yield quite similar results. Noticeable though is that under the locally parallel assumption the TS branch does cross over to the unstable half plane with an unstable range of axial wavenumbers, whereas, in the global setting the locally non-parallel base flow renders the global spectrum stable. As discussed in Ehrenstein and Gallaire [6], this is linked to the convective nature of the boundary layer flow. The damped branches are even more similar in the global and local settings, especially concerning the most damped branch which the mode m_3 is part of. Note that the wall normal

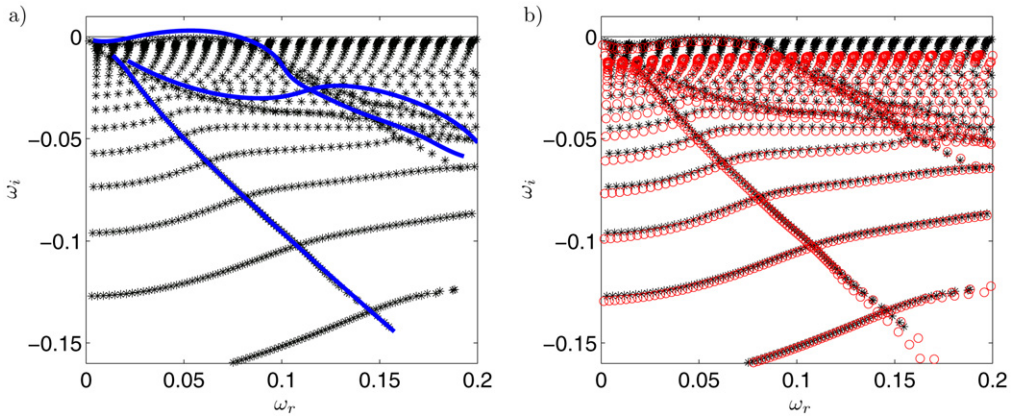

Fig. 4. (a) Solid lines trace three branches (the TS branch and two damped branches) of the spectra computed from the Orr–Sommerfeld equation when the wavenumber is varied continuously at $Re = 1374$. Stars show the spectra already depicted in Fig. 2. Notice that for the Orr–Sommerfeld equation the TS branch crosses over to the unstable half plane, whereas in the global setting, the non-parallel baseflow renders the global spectrum stable. (b) Comparison of spectra computed using the Robin boundary conditions (stars) and Dirichlet–Neumann (circles). One can see that the TS branch is slightly more damped using Dirichlet–Neumann. The continuous spectra is also more damped. Note that the discrete damped branches traced in (a) are not significantly affected by the change of boundary conditions.

shapes of the eigenfunctions are very similar in the global and local setting, but the global eigenfunctions are spatially evolving, growing as we move downstream.

Fig. 4(b) compares the global spectra obtained with the Robin boundary conditions and the spectra obtained using homogeneous Dirichlet at inflow and homogeneous Neumann conditions at outflow. Clearly the different boundary conditions gives different damping rates for the TS type of eigenmodes, but the frequency of the least stable TS eigenmode is the same. Later we will explain that the different damping rates do not affect how the different set of modes describe the dynamics of the flow in the interior of the domain. It can also be seen that the boundary conditions strongly influence the location of the eigenvalues in the complex plane as the Dirichlet–Neumann boundary conditions yield a more damped continuous branch. However, m_3 types of modes, associated with tilted damped modes of Blasius flow are not especially sensitive to the choice of boundary conditions.

2.2. *Convergence of optima*

The number of global two-dimensional temporal modes obtained depends strongly on the size of the Krylov subspace, and it may even depend on the value of the shift used in the shift and invert procedure. Further, the location of the eigenvalues in the complex plane seem to be somewhat sensitive to the boundary conditions used. However, we will now show that the optimal transient growth that may be retrieved from them are far more robust. By selecting only the TS type of modes, Ehrenstein and Gallaire [6] could obtain a growth in energy of one order of magnitude for $Re = 780$ and a box length of 500 for the propagating wavepacket. In this paper we will show that by adding the other types of modes, one obtains a much larger growth which is associated with the combination of the Orr mechanism [9] and the spatio-temporal growth of the wavepacket formed by TS wave type of structures. An important issue that is discussed is the convergence of the optimal growth results in terms of number of modes included in the expansion. We here take the tentative approach, gradually increasing the number of modes used to describe our flow state, searching for convergence. To our knowledge no analysis similar to that performed by Gustavsson [18] for the Orr–Sommerfeld equation has been published on the two-dimensional problem.

The total number of eigenvalues obtained by the Arnoldi method when using a Krylov subspace of size $m = 2000$ was 1205. For a given dimension of a Krylov subspace the Arnoldi method recovers converged eigenvalues contained within a circle of radius R around the shift value σ_0. Note that for this case the suitable shift value of $\sigma_0 = 0.08$ could be taken a priori from local theory, but within reasonable limits the choice of σ_0 is not crucial when working with such large Krylov subspaces. Increasing the Krylov subspace dimension is equivalent to drawing a larger circle in the complex space, where eigenvalues are obtained. The resulting eigenvalues hence satisfy

$$|\omega - \sigma_0| \leqslant R, \tag{12}$$

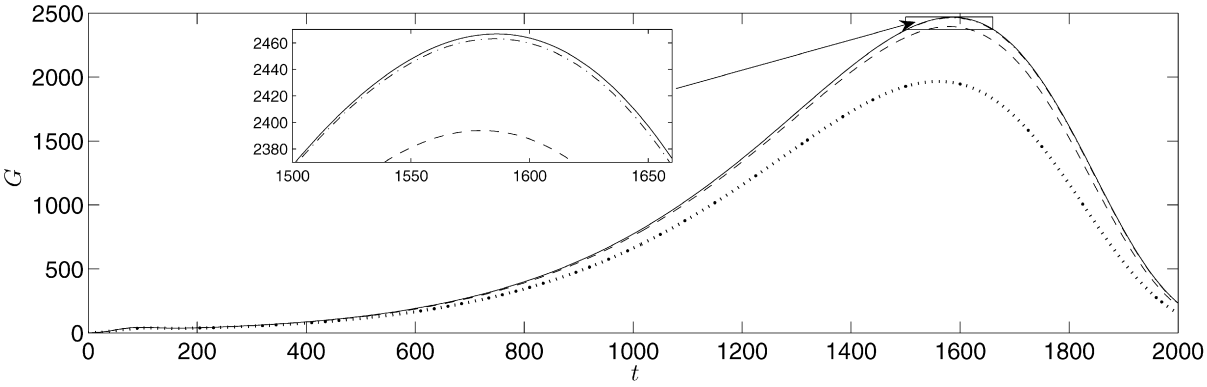

Fig. 5. Envelope of optimal growth for different Krylov subspace sizes. (...) corresponds to $R = 0.08$, (_ _ _) to $R = 0.1$ and (_ . _) to $R = 0.12$. The solid line shows the envelope including all modes obtained ($R = 0.16$). The inset shows a zoom at the maximum, indicating that the optimal growth is converged at $R = 0.12$. The kink in energy at time $t \approx 100$ will be explained together with Fig. 6.

where the radius R depends on how large the Krylov subspace is. Fig. 2 shows the radius resulting from three different Krylov subspace sizes on top of the spectra. The optimal growth envelope $G(t)$, as computed according to Eq. (7), obtained using different truncations is shown in Fig. 5. We stress that the envelope reveals at each instance of time the maximum possible amplification due to a specific initial condition, i.e. there are possibly different initial conditions leading to the specific growth at each instance of time. It is seen that a radius of $R = 0.08$, corresponding to 715 eigenmodes, is not sufficient to obtain converged results. A converging trend is seen for a radius of $R = 0.1$, corresponding to 854 modes, whereas for $R = 0.12$ (1014 modes) one may neglect the modification of the optimal growth envelope induced by a further increase of modes included in the optimization procedure. As mentioned earlier the spectra obtained when using Robin boundary conditions at inflow and outflow differed substantially in terms of damping rate ω_i from the spectra obtained using the Dirichlet–Neumann boundary conditions. In order to examine the influence of the different localization of eigenvalues in the complex plane we performed the optimal growth analysis using modes from both type of boundary conditions, truncating the basis at $R = 0.12$. Indeed we did find that the optimal initial condition obtained using both sets are identical and the subsequent time evolution remains exactly the same.

Cossu and Chomaz [3] was working on the model problem of Ginzburg–Landau mimicking convective growth. They conjectured that the more parallel the base flow becomes, the more non-normal the operator becomes and that consequently more modes are needed in order to locate optimal perturbations upstream. The flat plate boundary layer becomes more parallel with increasing Reynolds numbers. Indeed by performing the same convergence study for the lower Reynolds number of $Re = 500$ we observed convergence could be obtained already at a radius of $R = 0.08$, i.e. a small number of modes are needed.

3. Optimal initial condition

In the previous section we mentioned that it was possible to get a larger growth than that obtained when considering only the propagation of the TS type of wavepacket, and that this was due to the Orr mechanism. The thick solid line in Fig. 6 shows the envelope using an eigenmode expansion corresponding to a radius of $R = 0.12$ in a log scaling in order to emphasize the quick growth due to the Orr mechanism. Plotted as a thick dashed line in Fig. 6 is the envelope obtained when using only modes related to the TS instabilities, however multiplied by a factor of ≈ 20. This effectively means that one through the Orr mechanism has gained a factor of ≈ 20 compared to using only TS type of eigenfunctions. As earlier mentioned the envelope of the growth yields the maximum possible growth at each instance of time, with possibly different initial conditions leading to the optimal growth at different times. The thin solid line in Fig. 6 shows the actual energy evolution obtained by initializing the flow system with the structures leading to the global maximum growth at time $t = 1594$. The thin dash-dotted line shows the actual energy evolution of the disturbance leading to maximum energy growth at time $t = 98$. One can see that the optimal growth due to this pure Orr mechanism is a fast growing fast decaying disturbance. Note that the growth-factor as well as the corresponding optimal time ($t = 98$ and $E = 41.6$) are approximately twice as high as those provided by the local

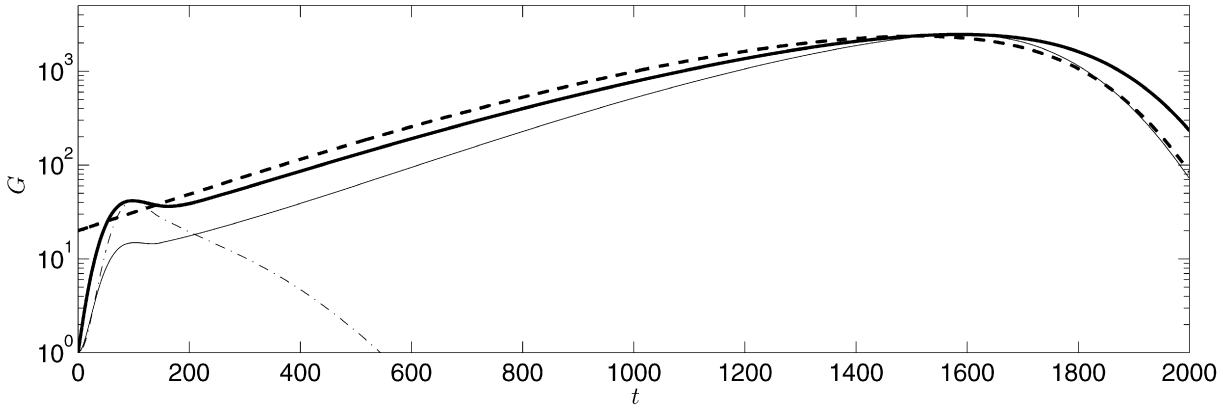

Fig. 6. Thick lines show envelopes of energy growth due to initial conditions. The thick solid line shows the envelope when using a Krylov subspace corresponding to $R = 0.12$ and the thick dashed line shows the envelope obtained when using only the TS type of modes in the optimization, magnified by a factor of 20, i.e. there is a gain of ≈ 20 in combining the Orr and TS mechanism. The thin lines shows actual energy evolution when initializing the flow system with the structures that leads to the maximum growth at time $t = 98$ (thin dash-dotted) and $t = 1594$ (thin solid).

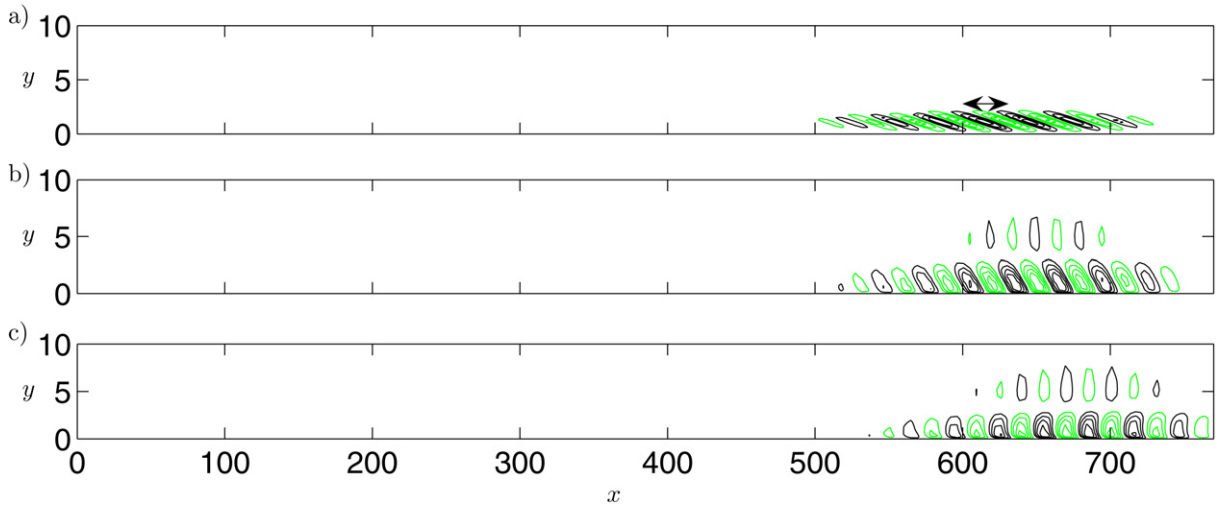

Fig. 7. Time evolution of streamwise velocity with the Orr mechanism at $Re = 1000$ leading to the energy evolution depicted as the thin dash-dotted line in Fig. 6. (a) Initial condition. (b) $t = 50$. (c) The maximum is located at $t = T = 98$ for which $E_T/E_0 = 41.6$. The double arrow in (a) shows the wave length of 25 as predicted by local theory.

analysis of Butler and Farrell [9] for a parallel Blasius boundary layer at $Re = 1000$ ($t = 45$ and $E = 28$). However, according to the time evolution of the streamwise velocity during the growth interval displayed in Fig. 7, it becomes clear, that comparison with the local theory should not be attempted using the inlet Reynolds number $Re = 1000$ but rather with a local Reynolds number representative of the location of the initial condition (using for instance the midpoint of the support of the initial perturbation, located at $x = 610$, this yields $Re = 1700$). We have therefore performed local optimal growth calculations based on a parallel Blasius boundary layers of displacement thickness 1.7 (corresponding to the local Reynolds number $Re = 1700$), yielding an optimal time $t = 120$ with corresponding optimal growth 34.8, closer to the result provides by the global optima. Note that there is no reason that the local results based on the parallel flow assumption should perfectly match with the global non-parallel computations. The corresponding optimal wavelength from local theory equals 25 and is depicted by an double arrow in Fig. 7(a), comparing favourably with the underlying wavelength in the wavepacket. Our local computations have further shown a tendency for the Orr mechanism of increasing optimal growth, increasing optimal time and increasing optimal wavenumber, when the boundary layer thickness and thereby the Reynolds number both increase. This tendency is clearly illustrated by Fig. 8 which shows for various box lengths, $L_x = 800, 600, 400$ for the different frames from

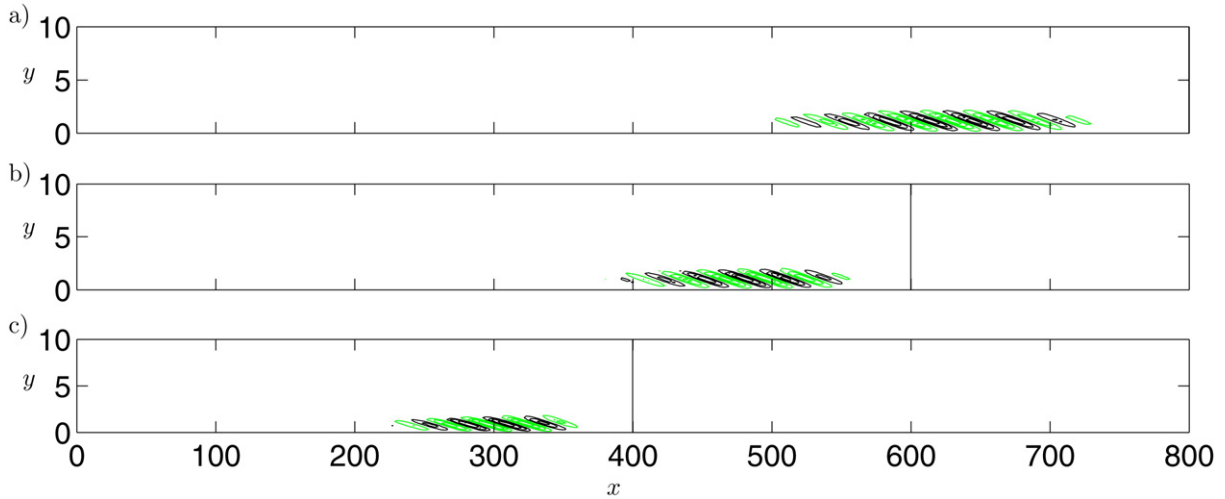

Fig. 8. Initial conditions corresponding to the pure Orr mechanism for different domain lengths. (a) $L_x = 800$, (b) $L_x = 600$ and (c) $L_x = 400$. The vertical lines indicates the end of the computational domain. The optimal initial condition is always located close to the outflow boundary, consistent with the prediction made in local analysis; namely that the Orr mechanism has increasing growth potential for increasing Reynolds number.

top to the bottom, that the optimal initial condition for this pure Orr mechanism is always located as far downstream as possible within the box. In contrast to the downstream located structures that yield the maximum growth for short times (see thin dash-dotted line in Fig. 6), the structures that leads to a large growth at larger times (see the thick line) are located far upstream as depicted in Fig. 9(a). The energy gain due to the upstream Orr mechanism is only half of that of the downstream located one (compare thin-solid and thin dash-dotted lines in Fig. 6, however as can be seen from Fig. 9 the disturbances gain energy through the Orr mechanism, after which they have the form of a TS type of wavepacket that propagates throughout the domain. The above results demonstrate that while the long-time behaviour of the disturbance is governed by the travelling wavepacket, its starting amplitude is optimized through the Orr mechanism.

4. Optimal forcing

Since boundary layers are convectively unstable, acting thereby as noise amplifiers, a preeminent role is played by the response to forcing, rather than by the detailed time-evolution of the initial condition, and the optimal forcing is therefore a relevant measure of the maximum possible growth that may be obtained in the box. While the evolution due to the optimal initial condition can be seen as a wave packet propagating, eventually leaving the computational box (or measurement section), the response from the flow to forcing will be persistent structures that at each streamwise station have a fixed amplitude, oscillating around the mean flow. In this section we are investigating the structure of the optimal forcing and the response at different frequencies. Fig. 10 shows the resolvent norm as defined in (11), where a large value indicates a large response to the given real frequency Ω. Note that the magnitude of the resolvent norm is both influenced by the distance $\mathrm{dist}\,(\boldsymbol{\Lambda} + \mathrm{i}\Omega\mathbf{I})$ in the complex plane to the eigenvalues and the condition number $\mathrm{cond}\,(\mathbf{F}) = \|\mathbf{F}\|_2\|\mathbf{F}^{-1}\|_2$ of the Cholesky factor of the energy measure. For normal operators the condition number is unity, hence the distance from an eigenvalue and the resolvent norm coincide. However, in our case the discretized dynamical matrix $\mathbf{A}$ is highly non-normal, so the condition number is considerably larger than unity. The dash-dotted line in 10 shows the gain due to the resonance effects associated with forcing close to an eigenvalue, whereas the thin solid line shows the gain obtained by including only TS type of modes in the optimization. When using a sufficient number of modes (corresponding to a radius $R = 0.12$ in the complex plane) we again observe a considerable increase in growth potential. The peak of the response for all cases is at the frequency $\Omega = 0.055$ and the streamwise component of the corresponding forcing structure is shown in the inserted frame in Fig. 10. Analogous to the optimal initial condition case, when using a sufficient number of modes in the optimization procedure Orr type of structures are produced, efficiently initializing TS waves. The optimal forcing structure is however more elongated

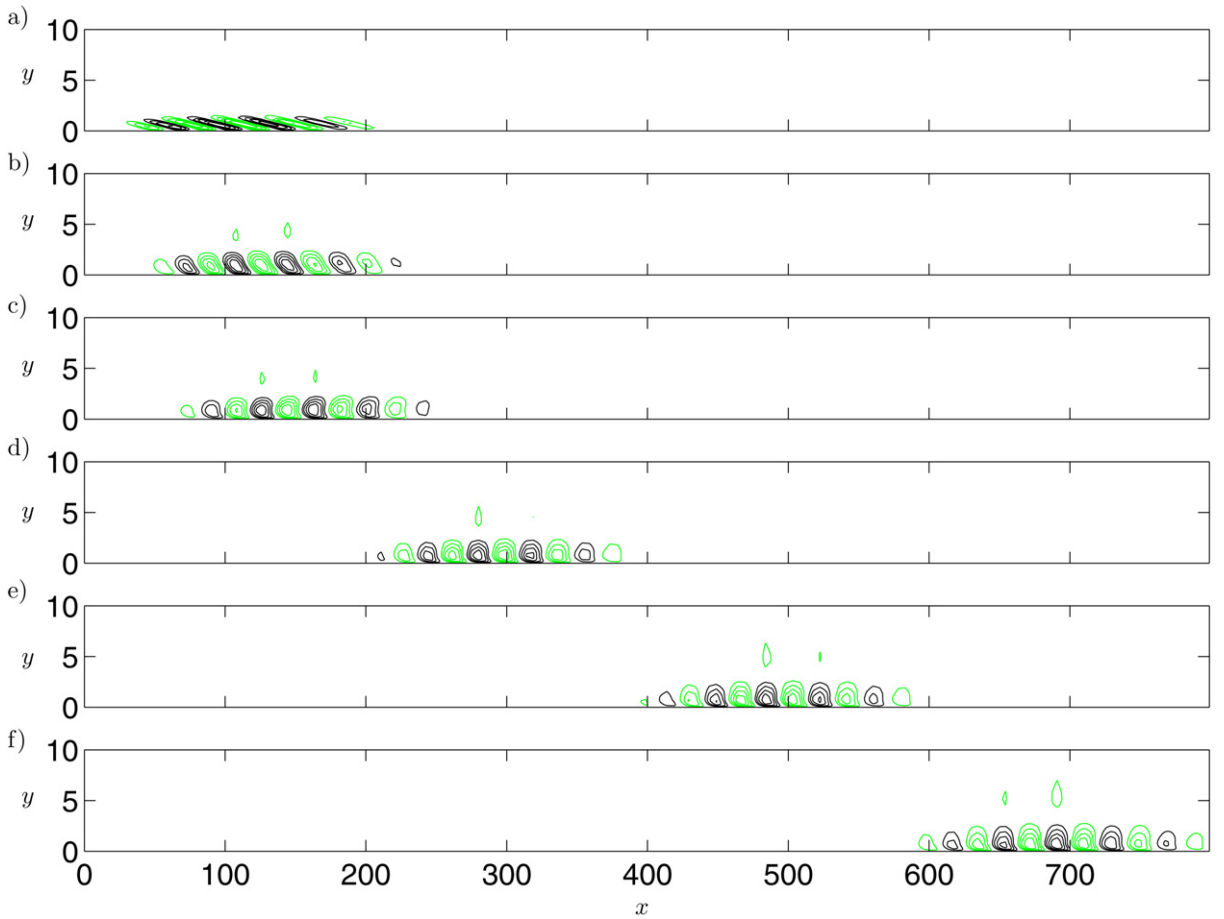

Fig. 9. Time evolution for streamwise velocity with the combined Orr and TS mechanism. Note that the amplitude is growing from frame to frame. (a) $t = 0$, maximum amplitude $A = 0.2$ (b) $t = 50$, $A = 0.38$ (c) $t = 100$, $A = 0.52$ (d) $t = 480$, $A = 1.0$, (e) $t = 960$, $A = 2.78$ and (f) $t = 1440$, $A = 5.8$.

in the streamwise direction than the optimal initial condition. The Orr mechanism provides a factor of five in gain compared to forcing only TS type of structures and a factor of 25 compared to exploiting pure resonant effects. The neutral point for this frequency (branch I) predicted by local theory is located at $x = 0$. We would expect the optimal forcing to be located in the vicinity of this neutral point, and indeed the forcing is located close to branch I. For lower frequencies we observe that the optimal forcing structures move further downstream and consist of longer wave lengths.

4.1. Direct numerical simulation results

A verification of the ability of the eigenmode system to capture the relevant dynamics of the flow is performed by applying the optimal forcing in DNS. For this purpose the real part of the optimal forcing device $\mathbf{q}_f \exp(-\mathrm{i}\Omega t)$ has been interpolated on the DNS grid and added as a forcing function to the Navier–Stokes system. The time evolution in the eigenmode system is given explicitly in terms of the expansion coefficients

$$\mathbf{k}(t) = -(\boldsymbol{\Lambda} + \mathrm{i}\Omega\mathbf{I})^{-1}\mathbf{k}_f\big(\exp(-\mathrm{i}\Omega t) - \exp(\boldsymbol{\Lambda} t)\big). \tag{13}$$

Note that Eq. (10) describes the asymptotic response of the system. Fig. 11 shows the pointwise energy integrated in the wall-normal direction, comparing the evolution in the DNS (solid lines) and the eigenmode system (dash-dotted lines). Snapshots are taken at times 80, 720, 1360 and 2000 with the amplitude growing as time increases. The response from the optimal forcing is the Orr mechanism followed by a TS wave. At time 2000 the disturbance has

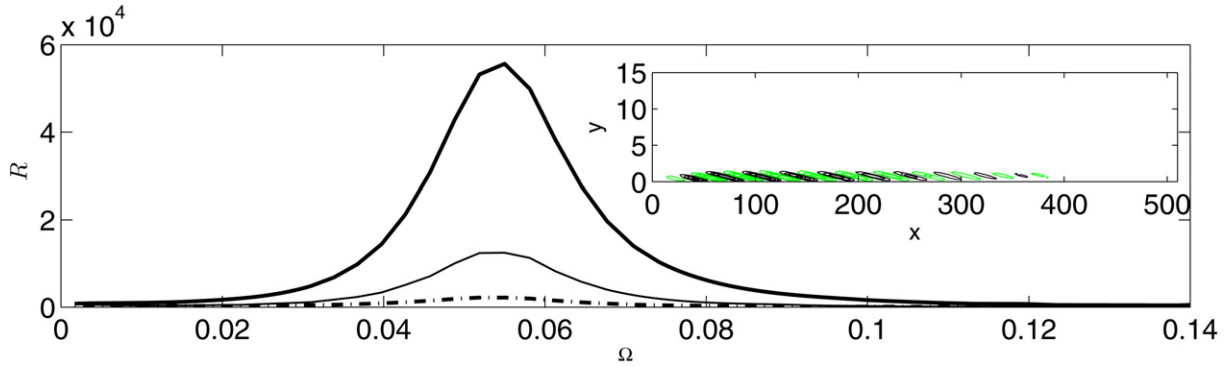

Fig. 10. Response to forcing at different frequencies. The thick line solid line shows the resolvent using a set of modes satisfying $|\omega - 0.08| < 0.12$. The thin solid lines shows the resolvent including only TS type of modes and the dash-dotted line shows the gain due to resonance. It is clear that one through non-normal effects have gained a factor of ≈ 25 (compare thick solid with dash-dotted line), whereas one through the Orr mechanism has gained a factor of ≈ 5 compared to using only TS type of modes. The peak response of all systems is at $\Omega = 0.055$. The inset shows the streamwise velocity component of the corresponding optimal forcing structure using all modes.

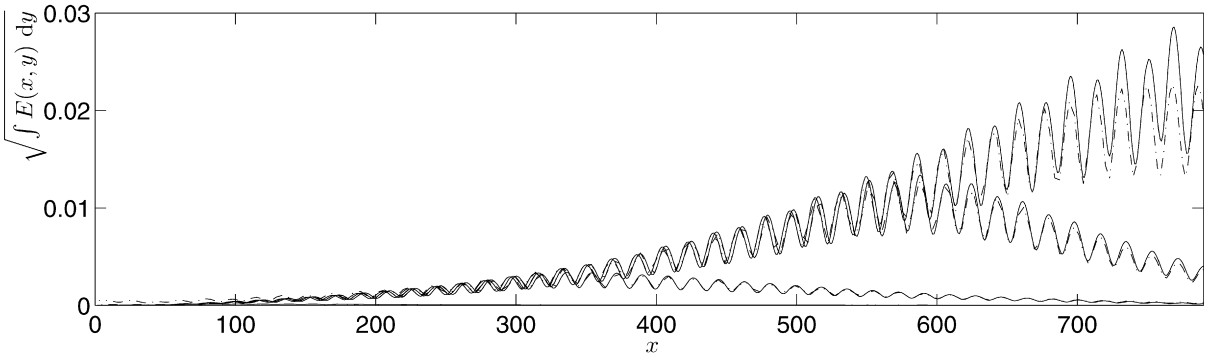

Fig. 11. Evolution of pointwise energy integrated in wall-normal direction at times 80, 720, 1360 and 2000. Solid lines shows DNS whereas dash-dotted shows eigenmode system. The amplitude is growing with increasing times. Note that at time 2000 the disturbance has filled the box and the energy reaches a threshold where TS waves occupy most of the domain. Note that the lines showing the integrated energy at time $t = 80$ are not visible due to their small amplitudes.

filled the box and the energy reaches a threshold where TS waves occupy most of the domain. The simple evaluation of 919 expansion coefficients yields an evolution in close agreement with the DNS, which for comparison has 1.5×10^6 degrees of freedom. At time 2000, even though the two systems are in phase an amplitude difference appears, most likely due to non-linear effects as well as to some possible weak reflections in the eigenmode system.

5. Conclusions

For highly non-parallel flows the validity of the local approach is questionable rendering the global eigenmodes the natural tool for stability analysis. If the flow under consideration is only slightly non-parallel local analysis may still provide correct results, but it is nevertheless interesting to establish the stability characteristics of the flow in terms of the global eigenmodes of the operator. The global eigenmodes provides the "full" description of the dynamics within the computational box. The Arnoldi method together with the shift and invert strategy locates the eigenmodes closest to the shift value within a radius in the complex plane given by the size of the Krylov subspace. The computed eigenmodes serve as a reduced basis in view of stability investigations, for which the basic procedure is to study features related to the pseudospectra, such as optimal initial conditions and optimal forcing. For the slightly non-parallel flow case studied here, many eigenmodes are needed in order to obtain converged results in terms of these measures. Both the optimal growth and optimal forcing analysis show that a combined effect of the Orr and TS-wave mechanism yields a large potential for downstream amplification in this convectively unstable regime. It is the

description of the upstream located tilted Orr structures that requires a large number of modes; the description of the TS waves only requires about 20 eigenmodes. Optimal forcing structures are applied both in the eigenmode system and in the DNS, and the subsequent time-evolutions in the two systems match very well. This confirms the robustness of optimally summing eigenmodes in order to bring out the important dynamics of the flow.

Acknowledgements

The authors would like to thank Matthieu Marquillie for providing the DNS code and Jérôme Hœpffner for fruitful discussions. Anatoli Tumin is acknowledged for suggestions on global/local spectrum comparisons.

References

[1] P. Huerre, P. Monkewitz, Local and global instabilities in spatially developing flows, Annu. Rev. Fluid Mech. 22 (1990) 473–537.
[2] E. Åkervik, J. Hœpffner, U. Ehrenstein, D.S. Henningson, Optimal growth, model reduction and control in a separated boundary-layer flow using global eigenmodes, J. Fluid Mech. 579 (2007) 305–314.
[3] C. Cossu, J. Chomaz, Global measures of local convective instability, Phys. Rev. Lett. 77 (1997) 4387–4390.
[4] J.M. Chomaz, Global instabilities in spatially developing flows: non-normality and nonlinearity, Annu. Rev. Fluid Mech. 37 (2005) 357–392.
[5] P.J. Schmid, D.S. Henningson, On the stability of a falling liquid curtain, J. Fluid Mech. 463 (2002) 163–171.
[6] U. Ehrenstein, F. Gallaire, On two-dimensional temporal modes in spatially evolving open flows: the flat-plate boundary layer, J. Fluid Mech. 536 (2005) 209–218.
[7] T. Ellingsen, E. Palm, Stability of linear flow, Phys. Fluids 18 (1975) 487–488.
[8] M.T. Landahl, A note on an algebraic instability of inviscid parallel shear flows, J. Fluid Mech. 98 (1980) 1–34.
[9] K.M. Butler, B.F. Farrell, Three-dimensional optimal perturbations in viscous shear flow, Phys. Fluids A 4 (1992) 1637–1650.
[10] S.C. Reddy, D.S. Henningson, Energy growth in viscous channel flows, J. Fluid Mech. 252 (1993) 209–238.
[11] L.N. Trefethen, A.E. Trefethen, S.C. Reddy, T.A. Driscill, Hydrodynamic stability without eigenvalues, Science 261 (1993) 578–584.
[12] P. Luchini, Reynolds-number-independent instability of the boundary layer over a flat surface: Optimal perturbations, J. Fluid Mech. 404 (2000) 289–309.
[13] P. Andersson, M. Berggren, D.S. Henningson, Optimal disturbances and bypass transition in boundary layers, Phys. Fluids 11 (1999) 134–150.
[14] T. Herbert, Secondary instability of boundary layers, Annu. Rev. Fluid Mech. 20 (1988) 487–526.
[15] M. Nayar, U. Ortega, Computation of selected eigenvalues of generalized eigenvalue problems, J. Comput. Phys. 108 (1993) 8–14.
[16] P.J. Schmid, D.S. Henningson, Stability and Transition in Shear Flows, Springer, 2001.
[17] N. Trefethen, M. Embree, Spectra and Pseudospectra the Behaviour of Nonnormal Matrices and Operators, Princeton University Press, 2005.
[18] L.H. Gustavsson, Initial value problem for boundary layer flows, Phys. Fluids 22 (1979) 1602–1605.